# A Potential Energy Shaping Controller with Ground Reaction Force Feedback for a Multi-Activity Knee-Ankle Exoskeleton

Nikhil V. Divekar[1], Jianping Lin[1], Christopher Nesler[2], Sara Borboa[3], and Robert D. Gregg[1,2]

***Abstract*— This paper presents the design and implementation of a novel multi-activity control strategy for a backdrivable knee-ankle exoskeleton. Traditionally, exoskeletons have used trajectory-based control of highly geared actuators for complete motion assistance. In contrast, we develop a potential energy shaping controller with ground reaction force (GRF) feedback that facilitates multi-activity assistance from a backdrivable exoskeleton without prescribing pre-defined kinematics. Although potential energy shaping was previously implemented in an exoskeleton to reduce the user's perceived gravity, this model-based approach assumes the stance leg is fully loaded with the weight of the user, resulting in excessive control torques as weight transfers to the contralateral leg during double support. The presented approach uses GRF feedback to taper the torque control output for any activity involving multiple supports, leading to a closer match with normative joint moments in simulations based on pre-recorded human data during level walking. To implement this strategy, we present a custom foot force sensor that provides GRF feedback to the previously designed exoskeleton. Finally, results from an able-bodied human subject experiment demonstrate that the exoskeleton is able to reduce muscular activation of the primary muscles related to the knee and ankle joints during sit-to-stand, stand-to-sit, level walking, and stair climbing.**

## I. INTRODUCTION

Every year more than 800,000 Americans are affected by stroke, out of which 200,000 are affected by hemiparesis of the lower limb [1]. Post-stroke rehabilitation typically involves gait training [2]. The most common, persisting gait deficit is foot-drop, which is associated with weakness in dorsi-flexors and/or co-contraction of plantar-flexors. Foot-drop in turn affects patients' foot clearance ability during swing, and also results in foot slap after heel contact. Another ankle deficit is plantar-flexor weakness during push-off, which is usually associated with more proximal compensation strategies to increase gait speed such as hip extension or increased plantar-flexion of the non-paretic leg. Improving ankle biomechanics is important because gait speed is a determining characteristic of functional tests [3].

Knee biomechanics are also affected in the hemiparetic gait [4]. Quadriceps weakness more often results in the adoption of a locked-knee gait, i.e., greater than normal extension or even hyper-extension of the knee during stance. This strategy is understandably used to avoid the issue of knee buckling upon heel contact. This compensatory mechanism however reduces gait velocity, and can also increase impact forces on the knee. Hamstring weakness can decrease the amount of foot clearance achieved during swing, resulting in compensatory mechanisms from proximal joints such as hip circumduction of the paretic leg or plantar-flexion of the unaffected leg, e.g., vaulting.

Robot assisted gait training (RAGT) has potential benefits over traditional, therapist-based rehabilitation [5]. First, RAGT can drastically increase the number of repetitions. Further, RAGT reduces the burden on the therapists, so more patients can be treated by a single therapist. Another advantage is that assistive joint torques can be applied in a more controlled and potentially customized manner. However, RAGT has not shown better outcomes compared to traditional therapist-based rehabilitation [6]. The current RAGT schemes enforce fixed joint trajectories on a patient, which may not match with a patient's innate trajectory before the stroke. Further, patient gait trajectories evolve towards a normative trajectory throughout the rehabilitation and re-learning process. Therefore, enforcing a particular trajectory may not be the best strategy to help a patient that may have different levels of impairment across the muscles. The second problem with this strategy is that it introduces patient complacency and greatly diminishes the stimulation and level of difficulty, ultimately reducing learning [7].

Recently, Goldfarb et al. [8] attended to this problem through the design of 1) a mobile exoskeleton (Indego) with backdrivable actuators to allow voluntary joint motion, and 2) a walking controller that does not depend on a pre-defined trajectory. The controller was designed to provide a combination of body-weight compensation and stance stabilization through the hip and knee actuators, because this exoskeleton did not have ankle actuators. However, the field of physical therapy supports the notion that the level of impairment on the hemiparetic side increases from proximal (hip) to distal (ankle), so distal joint recovery needs to be actively facilitated [9]. Further, [8] did not consider other activities of daily living (ADLs) that are necessary for regaining independence.

RAGT typically focuses on walking on a treadmill or level ground. However, stair climbing is an equally important ADL, and improvements gained in walking ability do not necessarily transfer to stair climbing [10]. This requires a different set of biomechanics and higher quadriceps and ankle involvement. Moreover, falling on stairs poses a disproportionately higher risk of severe injury or death in older adults [11]. Sit-to-stand is another activity that is typically

[1]Robotics Institute, [2]Department of Electrical Engineering and Computer Science, University of Michigan, Ann Arbor, MI 48109, USA. [3]Department of Mechanical Engineering, University of Texas at Dallas, Richardson, TX 75080, USA. Email: ndivekar@umich.edu, rdgregg@umich.edu

This work was supported by the National Science Foundation under Award Number 1652514 / 1949869. R. D. Gregg holds a Career Award at the Scientific Interface from the Burroughs Wellcome Fund. This work was also supported by a gift from The Philip R. Jonsson Foundation.

neglected in RAGT. Subjects greatly bias their weight to the non-paretic side when performing sit to stand [12], [13]. In fact, a lack of rehabilitation in sit-to-stand contributes to the increased fall risk in the post-stroke population [12]. Training ADLs with RAGT requires a mobile, backdrivable exoskeleton with a task-invariant controller that allows the patient to practice their preferred joint kinematics with proper torque assistance. Although progress has been made in the design of backdrivable exoskeletons [14]–[18], their control strategies still tend to be task specific.

To address these gaps, our prior work [15], [19] developed a task-invariant exoskeleton control strategy that assists the user's voluntary movements with energetic control objectives rather than kinematic objectives. This work implemented a control technique called potential energy shaping in a unilateral knee-ankle exoskeleton (Comex, Fig. 1(a)) to reduce the perceived gravity of the user. The control strategy leverages the exoskeleton's backdrivable, torque-controlled actuators, which comprise a high-torque motor with a low-ratio transmission (24:1). This design minimizes the backdrive torques (around 3 Nm) while being capable of output torques up to 60 Nm [14], which is sufficient for rehabilitation of the primary ADLs post-stroke [20], [21]. However, the potential energy shaping approach in [15], [19] relies on a model that assumes the stance leg is fully loaded with the weight of the user, resulting in excessive plantar-flexion torques as weight transfers from the assisted leg to the contralateral leg during double support. This excessive plantar-flexion can aggravate the foot-drop problem later in swing, during both walking and stair climbing. For sit to stand, the controller provides double the required torque, as body weight should be equally shared between the two legs. During sitting, excessive ankle and knee torques are applied as most of the weight is supported by the seat. These limitations must be overcome before this control approach can serve patient populations.

In this paper, we improve the potential energy shaping control method in Comex using ground reaction force (GRF) feedback to taper the torque control output for any activity involving multiple supports. We demonstrate feasibility with a single healthy subject performing a variety of tasks (walking, stair climbing, sit-to-stand, and stand-to-sit), resulting in reduced muscular effort when assisted by the exoskeleton. In Section II-A we briefly describe the dynamic model and control law of [19], which is improved with a GRF-based torque output tapering strategy. Section II-B describes the exoskeleton and custom foot force sensor used to implement the control strategy. Section II-C presents the methodology for the human subject experiment, which compares muscle activation between bare, passive, and active modes. Section III first uses pre-recorded human subjects data for level-ground walking to show the tapered torque outputs better match normative joint torques compared to the original control strategy. We then validate the foot sensor by comparing its measurements with a portable force plate. Moreover, the control strategy is implemented in the exoskeleton for experiments with a single healthy subject performing ADLs. Lastly, we perform a detailed inspection of the results in Section IV and discuss their bearing on future stroke studies in the closing remarks in Section V.

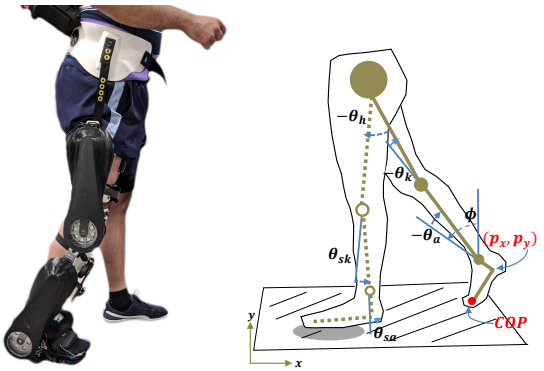


(a) (b)

Fig. 1. (a) Comex exoskeleton worn by a healthy user. (b) Kinematic model of the body reproduced from [22]. COP denotes the center of pressure, solid links denote the stance leg, and dashed links denote the swing leg.

## II. Methods

This section presents the theoretical framework for potential energy shaping with GRF-based tapering, the design of the exoskeleton and GRF force sensor, and the methods for the multi-activity human subject experiment.

### A. Potential Energy Shaping For Knee-Ankle Exoskeleton

*1) Model:* The biped model in Fig. 1(b) is restricted to the sagittal plane due to the planar actuation scheme of the exoskeleton. The masses of the human limb and the exoskeleton are combined together in the model. For control purposes, the dynamics of the stance and swing legs are modeled separately with coupled interaction forces. The generalized coordinates of the stance leg are given by $q_{st} = (p_x, p_y, \phi, \theta_a, \theta_k)^T \in \mathbb{R}^{5\times 1}$, where $(p_x, p_y)$ represents the Cartesian coordinates of the heel with respect to the inertial reference frame (IRF). The heel angle $\phi$ is defined with respect to the vertical axis, and $\theta_a$ and $\theta_k$ are the stance ankle and knee angles, respectively.

We use the Euler-Lagrange method to derive the dynamics of the stance leg, where the corresponding Lagrangian $L(q_{st}, \dot{q}_{st}) = K(q_{st}, \dot{q}_{st}) - V(q_{st})$ is the difference between the kinetic energy and potential energy [23]. The kinetic energy $K(q_{st}, \dot{q}_{st}) = \frac{1}{2}\dot{q}_{st}^T M(q_{st})\dot{q}_{st}$ is based on the generalized mass/inertia matrix $M(q_{st}) \in \mathbb{R}^{5\times 5}$, and $V(q_{st}) \in \mathbb{R}$ is the gravitational potential energy. In the following equations, we omit the arguments $q_{st}$ and $\dot{q}_{st}$ of the dynamic terms to abbreviate notation. Based on the Euler-Lagrange equation, the human-exoskeleton stance leg dynamics are given as

$$\frac{\mathrm{d}}{\mathrm{d}t}\partial_{\dot{q}_{st}} L - \partial_{q_{st}} L + A^T\lambda = M\ddot{q}_{st} + C\dot{q}_{st} + N + A^T\lambda = \tau, \quad (1)$$

where $C \in \mathbb{R}^{5\times 5}$ is the Coriolis matrix, $N = \nabla_{q_{st}} V \in \mathbb{R}^5$ is the gravitational forces vector, and matrix $A \in \mathbb{R}^{3\times 5}$ maps the ground reaction forces $\lambda \in \mathbb{R}^3$ onto the dynamics. We denote the torque inputs as $\tau = \tau_{exo} + \tau_{hum} = Bu + Bv + J^T F$, where $B = [0_{2\times 3}, I_{2\times 2}]^T \in \mathbb{R}^{5\times 2}$ maps the exoskeleton actuator torques $u \in \mathbb{R}^{2\times 1}$ and human muscle torques $v \in \mathbb{R}^{2\times 1}$ at

the knee and ankle onto the leg dynamics. The interaction forces $F \in \mathbb{R}^3$ between the hip and the swing leg are mapped to the system by the body Jacobian matrix $J$ [19].

For the swing leg model, the generalized coordinates are given as $q_{sw} = (h_x, h_y, \theta_{th}, \theta_{sk}, \theta_{sa})^T \in \mathbb{R}^{5\times 1}$, where $(h_x, h_y)$ are the positions of the hip with respect to the IRF, $\theta_{th}$ is the angle between the vertical axis and the swing thigh, and $\theta_{sk}$ and $\theta_{sa}$ are the swing knee and ankle angles, respectively. The swing leg dynamics have the same form as (1) except there is no ground contact, i.e., $\lambda = 0$.

*2) Control:* Our controller for the exoskeleton is based on the controlled Lagrangian method [24], which maps the original open-loop system to a desired closed-loop system (i.e., feedback system). We wish to achieve a closed-loop system with a modified potential energy $\tilde{V}$ as

$$M\ddot{q}_{st} + C\dot{q}_{st} + \tilde{N} + A^T\lambda = Bv + J^T F, \tag{2}$$

where $\tilde{N} = \nabla_{q_{st}}\tilde{V} \in \mathbb{R}^{5\times 1}$ represents the modified potential forces vector. Based on [24], systems (1) and (2) match if and only if there exists a full rank left annihilator of $B$ in the orthogonal projection form, i.e., $B^\perp B = 0$, such that

$$0 = B^\perp(N - \tilde{N}), \tag{3}$$

holds true along all trajectories $(q_{st}, \dot{q}_{st})$. Equation (3) is called the *matching condition* for potential energy [15]. The corresponding feedback control law is explicitly given by

$$u = (B^T B)^{-1} B^T (N - \tilde{N}), \tag{4}$$

which only depends on the configuration vector $q_{st}$ [19].

Given the left annihilator matrix

$$B^\perp = \begin{bmatrix} I_{3\times 3} & 0_{3\times 2} \\ 0_{2\times 3} & 0_{2\times 2} \end{bmatrix},$$

the matching condition (3) suggests the first three rows of the modified $\tilde{N}$ must be equal to those of $N$ [19]. To provide gravity compensation, we define the closed-loop potential forces vector as $\tilde{N} = [N_{1:3}^T, \mu \cdot N_{4:5}^T]^T$, where $N_{i:j}$ contains the $i$th to $j$th elements of the vector $N$, and $\mu$ is a constant scaling coefficient. The resulting control law only depends on the foot orientation, ankle angle, and knee angle. The coefficient $\mu$ is selected to be less than one so that the exoskeleton compensates for a fraction of the gravitational torques at the ankle and knee joints, providing virtual body-weight support (BWS). The controller for swing period is derived in a similar manner using the swing leg coordinates [19].

Note the model (1) does not know the state of the contralateral leg, and it is practically impossible to measure the interaction forces $F$ between the hip and swing leg. Hence, the potential energy shaping controller compensates for a fraction of the full body weight during stance, even when part of the body weight is supported by the other leg or a chair. We attend to these issues by implementing a GRF-based torque tapering strategy, where a scaling factor $\varepsilon$ multiplies the exoskeleton torque commands from (4) during the stance phase. The scaling factor $\varepsilon$ is a function of the vertical ground reaction force measured by a custom force sensor in the Comex foot plate, which is described next.

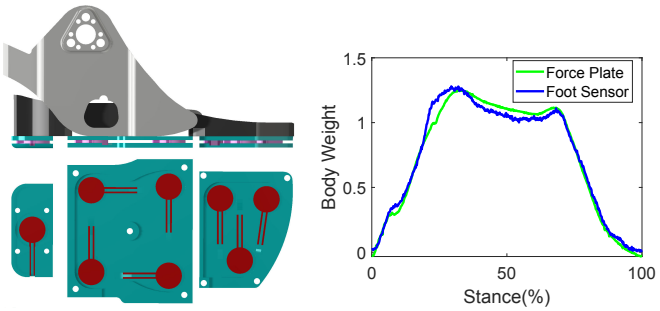


(a) (b)

Fig. 2. (a) Sagittal view of Comex foot plate (top) shows the rigid structure (gray), insole (black), force sensor plates (green), and force-channeling pucks (purple). Top-down view (bottom) shows the layout of FSRs (red) within the sensor plates (green). (b) Comparison of simultaneously recorded foot sensor and force plate readings for one stance period during level-ground walking. Both signals are normalized to body weight and temporally normalized to percent stance period. A correlation coefficient of 0.99 and a mean squared error of 0.03 were found between the two signals.

### *B. Mechanical Design of Exoskeleton and GRF Sensor*

The partial-assist device (Comex [14], [15]) for which the controller is designed is shown in Fig. 1(a). The device can produce 30 Nm continuous torque (60 Nm peak) at the knee and ankle using 200 W frameless BLDC motors (Emoteq) with a 24:1 transmission ratio. The transmission comprises a belt stage and a custom planetary gearbox inside the driven sprocket. The motors are driven with sinusoidal commutation by Elmo Gold Twitter drives (rated to 30 A). The control system includes the onboard sensors and computation needed to implement torque control laws, including Sunrise torque sensors for closed-loop torque control running at 800 Hz on a National Instruments myRIO microcontroller. High-resolution relative encoders measure joint angles/velocities, and a 6-axis Microstrain IMU measures orientation. The system is powered by an onboard Lithium-Ion battery pack. The unpowered backdrive torque is about 3 Nm, allowing the user to freely control their joint kinematics. The device weighs about 4.5 kg and includes safety features such as hard stops and current limiters at both joints.

The foot sensor was designed to record the wearer's vertical ground reaction force with the accuracy of a force plate, while maintaining the profile and level of portability necessary to incorporate into the underfoot region of Comex's footplate (Fig. 2(a)). This was accomplished using a structure inspired by force plate construction, wherein each section includes two rigid plates, held apart by circular spacers (pucks) that each sit atop a FlexiForce A401 (Tekscan, South Boston, MA) force sensitive resistor (FSR). Due to the gap between the rigid plates being held open by the pucks, all force applied to the plates' large surface areas travels through the pucks and, as a result, the FSRs. A thin layer of compressible foam is placed above and below the FSRs to ensure sufficient pressure distribution between the puck and the lower plate. By funneling the force to the FSRs in this manner, we are able to avoid having large portions of the foot which do not transmit their force to a sensor due to their lack of surface area coverage. This is an issue

that can also be addressed by using FSR-style sensors with large surface areas (e.g., Tekscan F-Scan), but high cost and limited durability keep this from being an ideal solution.

The FSRs from the heel and middle section of the sensor are connected to each other in parallel and form the total heel resistance. Similarly, the 3 FSRs from the toe section are connected in parallel, forming the total toe resistance. The change in resistance of the heel and toe (related to the force being applied at these locations) is sensed and amplified by an operational amplifier circuit recommended in the Tekscan data sheet [25]. This circuit also linearizes the nonlinear resistance-force relationship. Finally, MyRIO software is used to calibrate the sensors before each experiment to achieve a final readout normalized to body weight.

### C. Human Subject Experiment Methodology

The human subject experiment was designed to demonstrate the potential benefit of the knee-ankle exoskeleton during multiple, common ADLs. These tasks were: sit to stand, stand to sit, treadmill walking, and stair climbing. The primary aim of the experiment was to show a reduction in effort of the muscles related to the joints assisted by Comex. We assessed activation levels of the following muscles: vastus medialis oblique (VMO), biceps femoris (BF), tibialis anterior (TA), and soleus (SOL), which function as a knee extensor, knee flexor, dorsi-flexor, and plantar-flexor respectively. A single, male human subject (mass: 80 kg, height: 1.78 m) was enrolled for the study, which was approved by the Institutional Review Board at the University of Texas at Dallas and the University of Michigan.

The sit to stand, and stand to sit tasks were completed as part of a repetitive sit-stand cycle which consisted of four phases: sitting, sit to stand, standing, and stand to sit. Each phase lasted 1.5 s (cued using a metronome set to 40 BPM). A total of nine repetitions were carried out for each of the three modes tested: bare (without exoskeleton), passive (exoskeleton un-powered), and active (exoskeleton assistance). The subject was instructed to maintain the same sit-stand technique for all three modes to minimize any bias in the results. The next task performed was level walking on a treadmill. The walking speed and cadence were kept the same for all three modes, and were set to the subject's self selected levels (speed of 2 MPH and cadence of 75 steps/min). These were determined while the subject walked with Comex on passive mode. Feedback of the selected cadence was provided using a metronome, and the subject was asked to comply with it to the best of his ability. A total of 30 gait cycles were collected for each of the three modes tested. While the subject was allowed to use the treadmill handle bars during practice, this was disallowed during the trials which were recorded. The last task tested was stair climbing. An internal staircase of the building housing the laboratory was used for this purpose. Data was collected in two sets for each mode, where each set consisted of climbing up the full staircase acquiring four gait cycles. Thus eight gait cycles were collected for each of the three modes. A metronome set at 40 BPM was provided to help the subject keep the cadence

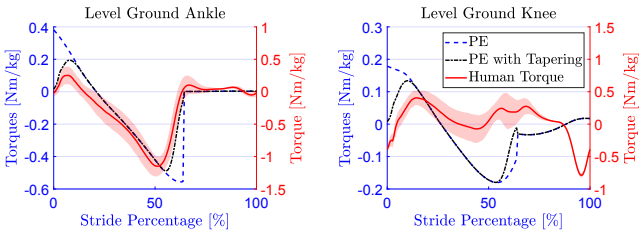


Fig. 3. Exoskeleton torques for potential energy (PE) shaping without (blue dashed) and with (black dash-dot) tapering, based on zero incline treadmill walking data at 1.0 m/s. The red solid lines represent mean human torques, and the shaded region about the mean represents $\pm 1$ standard deviation. Positive values represent ankle dorsi-flexion torques and knee extension torques. Note that the scales of the left axis (exoskeleton assistance torques) and right axis (normative human torques) are different for ease of comparison.

consistent. While this cadence is lower than the average for healthy subjects, this ensured longer muscle loading times to better distinguish the effect of Comex assistance, and also is closer to the low cadence of stroke patients who are the intended end users of the device. For all tasks, the level of assistance was set to $\mu = 0.83$ and $\mu = 0.6$ for stance and swing respectively for the active mode, which was based on the comfort level of the subject during initial practice.

We used a Delsys system to acquire electromyography (EMG) data from the four muscles VMO, BF, TA, and SOL of the right limb (the side with Comex). The skin was appropriately prepared to reduce skin-electrode impedance. An inter-electrode distance of 10 mm was used. EMG data corresponding to each sit to stand, and stand to sit repetition was cropped based on the deflection and return to steady state of the sagittal femur angle (measured using an accelerometer built into the EMG sensor). The level walking and stair climbing trials were cropped into gait cycles using spikes in the accelerometer data corresponding to heel strike. All data was normalized with respect to the maximum peak of the ensemble averages (across repetitions) of the three modes (bare, passive, active) [26]. This was done for each task, and muscle separately, resulting in the signals being converted to a percentage of the maximum voluntary contraction level (%MVC). The normalized trials were then integrated with respect to time to represent muscular effort as %MVC.s.

## III. Results

### A. Tapering Simulation Using Normative Kinematic Data

In this simulation, we examine the exoskeleton torques provided by inputting normative human kinematic data during level-ground walking [27] into the controller (4). We set the scaling factor $\varepsilon = \sin(\frac{f}{f_{bw}} \cdot \frac{\pi}{2})$, which multiplies the exoskeleton torques during the stance phase, where $f$ represents the vertical ground reaction force measured by the force plate, and $f_{bw}$ represents the weight of the human subject. Once $f$ reaches $f_{bw}$, the scaling factor becomes one, and the whole body weight acts on the contact foot. The reason for setting $\varepsilon = \sin(\cdot)$ is to have a smooth transition when $f$ is around $f_{bw}$.

Fig. 3 compares the simulated exoskeleton joint torques with normative joint torques for treadmill walking [27]. Re-

sults show that potential energy shaping with tapering better matches the human torque profiles than without tapering, suggesting the tapering strategy will deliver more appropriate assistance in the subsequent experiments with ADLs.

### B. Foot Sensor Validation

The foot sensor design was validated by wearing Comex during overground walking, in which the wearer stepped on a portable force plate (Kistler). The foot sensor (via myRIO) and force plate recordings were started and stopped at the same time, and sampled at the same rate. The data in Fig. 2(b) were trimmed to contain just the stance phase of the step on the force plate, and normalized using the subject's body weight. This trial resulted in a correlation coefficient of 0.99 between the foot sensor and force plate data (taken as gold standard), with a mean square error (MSE) of 0.03 between the two signals. Further analysis of the graph shows that the difference between the peaks in both signals is negligible, showing the linear behavior of the developed force sensor.

### C. Experiments with Activities of Daily Living

The primary objective of the human subject experiment was to determine the effect of Comex assistance torques on the muscles related to the knee and ankle joint movements during the four tested tasks. Fig. 4 shows the ensemble average (across repetitions) of time-normalized EMG for all muscles (VMO, BF, TA, and SOL), tasks (sit to stand, stand to sit, level walking, and stair climbing), and exoskeleton modes (bare, passive, and active). Also shown are the simultaneously recorded exoskeleton assistance torques pertaining to the muscles (knee torques are overlaid for VMO and BF, whereas ankle torques are overlaid for TA and SOL). Generally during active mode, a reduction in agonist EMG (agonist muscular activation) was observed during periods of higher torque assistance levels of the related joint compared to bare and passive modes. A detailed analysis of Fig. 4 is given in Section IV where we dissect the EMG patterns found for the various phases of the tasks. We show quantitative comparisons of mean muscular effort for the various tasks and muscles in Tables I-IV.

TABLE I

EFFORT COMPARISONS FOR SIT TO STAND: SHOWING MEAN (± SD) FOR MUSCLES (COLUMNS) AND MODES (ROWS).

| Effort [%MVC.s] | VMO | BF | TA | SOL |
|---|---|---|---|---|
| Bare | 78.8 (6.2) | 86.0 (8.8) | 63.2 (15.2) | 33.6 (8.2) |
| Passive | 67.6 (7.9) | 96.9 (15.3) | 54.7 (7.9) | 46.4 (10.9) |
| Active | 34.1 (3.9) | 61.6 (8.6) | 30.0 (4.3) | 49.7 (9.7) |

TABLE II

EFFORT COMPARISONS FOR STAND TO SIT: SHOWING MEAN (± SD) FOR MUSCLES (COLUMNS) AND MODES (ROWS).

| Effort [%MVC.s] | VMO | BF | TA | SOL |
|---|---|---|---|---|
| Bare | 98.8 (13.6) | 93.8 (11.6) | 85.2 (13.8) | 59.2 (14.1) |
| Passive | 87.4 (7.2) | 72.1 (7.4) | 85.9 (9.4) | 68.4 (16.8) |
| Active | 51.1 (5.2) | 47.1 (7.0) | 50.0 (10.8) | 48.5 (7.5) |

TABLE III

EFFORT COMPARISONS FOR WALKING: SHOWING MEAN (± SD) FOR MUSCLES (COLUMNS) AND MODES (ROWS).

| Effort [%MVC.s] | VMO | BF | TA | SOL |
|---|---|---|---|---|
| Bare | 10.4 (9.3) | 23.8 (11.1) | 32.3 (3.6) | 42.9 (5.4) |
| Passive | 62.7 (6.1) | 25.0 (3.0) | 54.4 (4.7) | 46.4 (2.8) |
| Active | 71.9 (7.2) | 38.8 (6.9) | 44.6 (4.7) | 26.3 (2.2) |

TABLE IV

EFFORT COMPARISONS FOR STAIRS: SHOWING MEAN (± SD) FOR MUSCLES (COLUMNS) AND MODES (ROWS).

| Effort [%MVC.s] | VMO | BF | TA | SOL |
|---|---|---|---|---|
| Bare | 73.0 (9.9) | 102.3 (15.6) | 73.3 (15.9) | 96.5 (12.8) |
| Passive | 82.6 (12.8) | 137.7 (11.2) | 104.9 (10.7) | 64.7 (11.9) |
| Active | 50.9 (4.1) | 111.4 (10.8) | 87.3 (10.6) | 56.6 (5.6) |

## IV. DISCUSSION

The main objective of this paper was to demonstrate the efficacy of a task-invariant controller for a backdrivable knee-ankle exoskeleton in providing partial assistance during multiple ADLs. Our previous work had established the theoretical basis for energy shaping control of exoskeletons [15]. In Section II-A we revisited the potential energy shaping controller and highlighted a solution for multi-support phases of ADLs. In Section III-A, we showed via simulation that scaling (or tapering) its torque output with the vertical GRF results in more normative joint moments for level walking. A similar case can be made for the other ADLs, including sit-stand transitions and stair climbing. In Sections II-B and III-B we showed the implementation of a FSR-based foot force sensor for tapering.

Using Comex with the improved control scheme and custom force sensor, we presented the effects of partial-assistance on muscular activation (EMG) across multiple ADLs. While EMG plots of all muscles tested have been shown for all tasks performed, we discuss the more biomechanically meaningful results below. Potential energy shaping (which is a position based control strategy) is highly suited for assisting in tasks with slower dynamics, such as sit to stand and stand to sit. These two tasks primarily require knee extension, hip extension, and dorsi-flexion torques [28]. During sit to stand these occur in the form of concentric contractions, and during stand to sit, as eccentric contractions. Accordingly, we found large reductions in VMO (knee extensor), BF (hip extensor), and TA (dorsi-flexor) activations for active mode in both these tasks when compared to bare and passive modes (see Tables I and II for mean effort values). Accordingly, the reductions in activations were aligned with the period of higher exoskeleton assistance torques as can be seen in Fig. 4. The reduction in BF activation is interesting, as no direct hip assistance torque was provided. However, we attribute this to an indirect effect on hip moment, possibly due to a change of strategy to a more knee dominant one. Another role of BF is in creating a knee flexion moment, and its co-contraction along with VMO acts to stabilize the knee

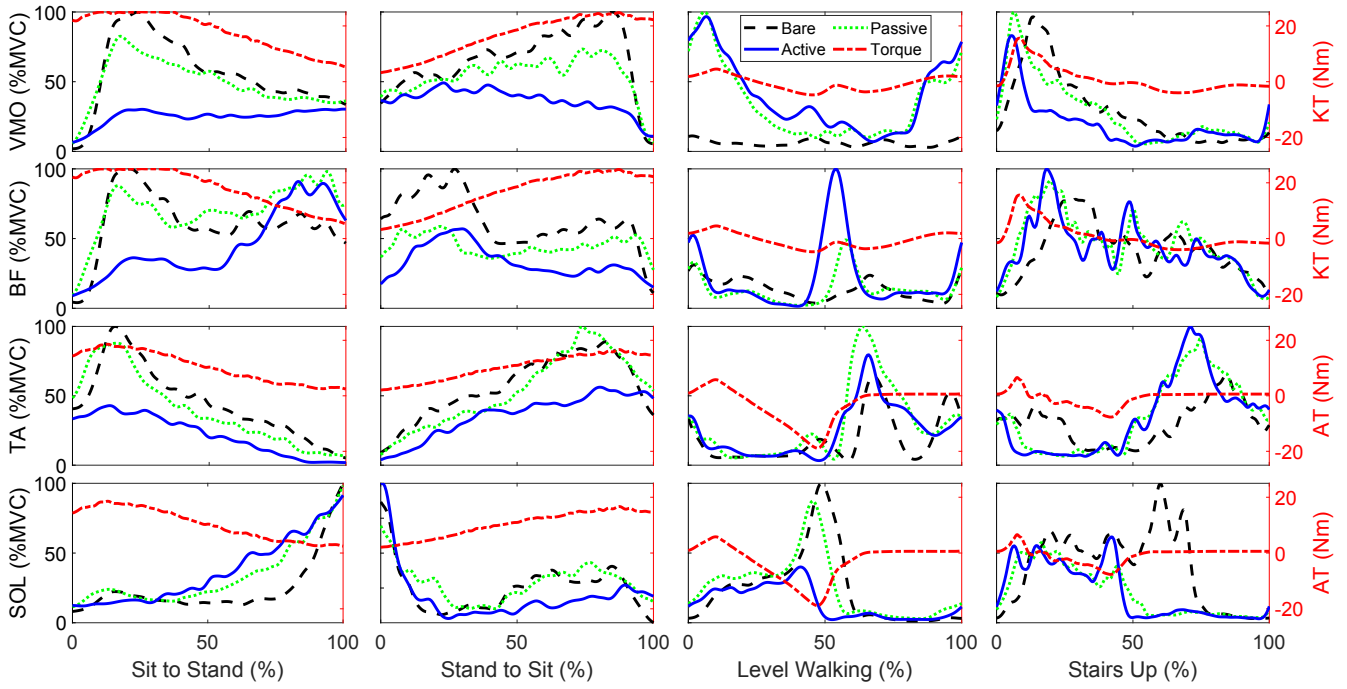


Fig. 4. Comparisons of mean EMG between the three exoskeleton modes tested (bare, passive, and active), along with the assistance torque for the corresponding joint. The four activities tested (sit to stand, stand to sit, level walking, and stairs up) are shown column wise, whereas the four muscles tested (VMO, BF, TA, and SOL) are shown row wise. Rows one and two represent the muscles primarily responsible for controlling the knee joint and torque provided by Comex at the knee (KT). Rows three and four represent the muscles primarily responsible for controlling the ankle joint and the torque provided by Comex at the ankle (AT). A positive KT represents a knee extension torque, whereas a positive AT represents a dorsi-flexion torque.

joint. Therefore, another explanation could be the reduced need to stabilize the knee joint with exoskeleton assistance. Generally, agonist-antagonist co-contraction is higher for a more difficult task [29], which was likely reduced due to the decreased difficulty in active mode.

Stair climbing during stance has similar biomechanics to sit-to-stand, whereby knee extension, hip extension, and dorsi-flexion torques are required during early to mid stance to elevate the body's center of mass [30]. Additionally, a plantar-flexion torque during late stance is used to push off as in level walking [30]. Accordingly, we found reductions in VMO and TA activations during early to mid stance, and a decrease in SOL activation during late stance (see Table IV for mean effort values). Comex provided knee flexion torques during swing to help raise the shank, and is the likely cause of the reduction seen in BF EMG for active mode during early to mid swing (Fig. 4). Overall, reductions in muscle activations aligned with the respective assistance torques, showing the contribution of Comex towards the net joint torques.

Level walking has the fastest dynamics out of the four tasks tested, and as such, a potential energy shaping control scheme that is based purely on joint angular positions (and not on velocity) has reduced benefits compared to the slower tasks, e.g., sit to stand. The knee joint kinematics in early stance change rapidly in response to the impact of heel strike, but the change in knee angle is relatively small [31]. In this case, the quadriceps primarily work to counteract momentum rather than the effect of gravity. Although Comex did provide a mild supportive knee extension torque during early stance (Fig. 4), this did not translate to a reduction in VMO activation with the particular subject. A possible explanation for this is that the subject changed his gait to walk with a locked knee during bare mode, leading to minimal VMO activation. During passive and active modes, his VMO activation was much higher than bare. This is likely due to the weight of Comex significantly increasing the momentum of the swing leg before heel strike, which needed to be countered by the VMO.

The assistance torque at the ankle is of a significantly larger magnitude compared to the knee during walking (Fig. 4), and therefore we expected to find beneficial effects for this joint. Indeed a large reduction in SOL activation was found during pushoff for active mode, which aligns well with the delivery of the plantar-flexion assistance torque. Interestingly, the assistance dorsi-flexion torque provided during early stance did not result in a significant reduction in TA activation in this phase. However, the dorsi-flexion torques provided during swing (to assist with foot clearance), did translate to a reduction in TA activation for active mode compared to passive mode, but not compared to bare mode. The likely reason for this is that dorsi-flexion assistance torques during swing are less than 1 Nm in amplitude, which is less than the backdrive torque of 3 Nm; therefore the difference in activation is likely only found with respect to passive mode. Table III provides mean effort values for the walking task, where we see only SOL had an overall mean effort reduction, when we consider the full gait cycle.

## V. Conclusion and Future Work

This paper demonstrated the possible benefits of potential energy shaping control with GRF tapering in a backdrivable knee-ankle exoskeleton for assisting multiple ADLs. The controller provided holistic reductions in lower-limb muscular activation for tasks with slower dynamics (e.g., sit-stand transitions). Substantial assistance was provided to the plantar-flexors during pushoff in level walking and to the quadriceps during stance in stair climbing. Further testing is needed on a larger cohort of subjects to verify the control behavior on a broader range of gait patterns. Additionally, assistance to the swing phase during level walking should be improved, e.g., by compensating for the backdrive torque in the torque command. Lastly, we will validate a total energy shaping controller that accounts for joint velocities [32], so that tasks with faster dynamics can be better supported. The final purpose of the exoskeleton is for stroke rehabilitation, where the goal is to augment the muscle forces (rather than reduce muscle activation) in order to restore normative kinematics and associated performance metrics (e.g., gait speed). By aligning with normative human torques, the exoskeleton torques that reduced muscle effort in a healthy individual in this study could instead enhance weakened joints in a future stroke study.

## ACKNOWLEDGMENT

The authors thank Vamsi Krishna Peddinti, Kayla Sheppodd, Cally Soh, and Kaci Le for their assistance.

## References

[1] V. Ma, L. Chan, and K. Carruthers, "Incidence, prevalence, costs, and impact on disability of common conditions requiring rehabilitation in the US: Stroke, spinal cord injury, traumatic brain injury, multiple sclerosis, osteoarthritis, rheumatoid arthritis, limb loss, and back pain," *Arch. Phys. Med. Rehab.*, vol. 95, no. 5, pp. 986–995, 2014.

[2] G. Morone, S. Paolucci, A. Cherubini, D. De Angelis, V. Venturiero, P. Coiro, and M. Iosa, "Robot-assisted gait training for stroke patients: current state of the art and perspectives of robotics," *Neuropsychiatric disease and treatment*, vol. 13, p. 1303, 2017.

[3] K. K. Patterson, W. H. Gage, D. Brooks, S. E. Black, and W. E. McIlroy, "Changes in gait symmetry and velocity after stroke: a cross-sectional study from weeks to years after stroke," *Neurorehabilitation and Neural Repair*, vol. 24, no. 9, pp. 783–790, 2010.

[4] S. M. Woolley, "Characteristics of gait in hemiplegia," *Topics in Stroke Rehabilitation*, vol. 7, no. 4, pp. 1–18, 2001.

[5] K. van Kammen, A. M. Boonstra, L. H. van der Woude, H. A. Reinders-Messelink, and R. den Otter, "Differences in muscle activity and temporal step parameters between lokomat guided walking and treadmill walking in post-stroke hemiparetic patients and healthy walkers," *J. NeuroEng. Rehabil.*, vol. 14, no. 1, p. 32, 2017.

[6] B. H. Dobkin *et al.*, "Methods for a randomized trial of weight-supported treadmill training versus conventional training for walking during inpatient rehabilitation after incomplete traumatic spinal cord injury," *Neurorehab. Neural Repair*, vol. 17, no. 3, pp. 153–167, 2003.

[7] N. C. Bejarano, S. Maggioni, L. De Rijcke, C. A. Cifuentes, and D. J. Reinkensmeyer, "Robot-assisted rehabilitation therapy: recovery mechanisms and their implications for machine design," in *Emerging Therapies in Neurorehabilitation II*. Springer, 2016, pp. 197–223.

[8] S. A. Murray, K. H. Ha, C. Hartigan, and M. Goldfarb, "An assistive control approach for a lower-limb exoskeleton to facilitate recovery of walking following stroke," *IEEE Trans. Neural Syst. Rehabil. Eng.*, vol. 23, no. 3, pp. 441–449, 2015.

[9] A. A. Sheila Lennon, David Baxter, "Physiotherapy based on the bobath concept in stroke rehabilitation: a survey within the UK," *Disability and Rehabilitation*, vol. 23, no. 6, pp. 254–262, 2001.

[10] G. Morone, M. Matamala-Gomez, M. V. Sanchez-Vives, S. Paolucci, and M. Iosa, "Watch your step! who can recover stair climbing independence after stroke?" *Eur. J. Phys. Rehabil. Med.*, vol. 54, no. 6, p. 811—818, 2018.

[11] J. V. Jacobs, "A review of stairway falls and stair negotiation: Lessons learned and future needs to reduce injury," *Gait & posture*, vol. 49, pp. 159–167, 2016.

[12] B. Amira, P. France, D. Patrick, and N. Sylvie, "Determinants of sit-to-stand tasks in individuals with hemiparesis post stroke: A review," *Ann. Phys. Rehab. Med.*, vol. 58, no. 3, pp. 167 – 172, 2015.

[13] D. S. Marigold and J. J. Eng, "The relationship of asymmetric weight-bearing with postural sway and visual reliance in stroke," *Gait & posture*, vol. 23, no. 2, pp. 249–255, 2006.

[14] H. Zhu, J. Doan, C. Stence, G. Lv, T. Elery, and R. Gregg, "Design and validation of a torque dense, highly backdrivable powered knee-ankle orthosis," in *IEEE Int. Conf. Robot. Autom.*, 2017, pp. 504–510.

[15] G. Lv, H. Zhu, and R. D. Gregg, "On the design and control of highly backdrivable lower-limb exoskeletons," *IEEE Control Systems Magazine*, vol. 38, no. 6, pp. 88–113, 2018.

[16] J. Wang, X. Li, T.-H. Huang, S. Yu, Y. Li, T. Chen, A. Carriero, M. Oh-Park, and H. Su, "Comfort-centered design of a lightweight and backdrivable knee exoskeleton," *IEEE Rob. Autom. Lett.*, vol. 3, no. 4, pp. 4265–4272, 2018.

[17] S. Yu, T.-H. Huang, D. Wang, B. Lynn, D. Sayd, V. Silivanov, Y. S. Park, Y. Tian, and H. Su, "Design and control of a high-torque and highly backdrivable hybrid soft exoskeleton for knee injury prevention during squatting," *IEEE Rob. Autom. Lett.*, vol. 4, no. 4, pp. 4579–4586, 2019.

[18] H. Zhu, C. Nesler, N. Divekar, M. Ahmad, and R. Gregg, "Design and validation of a partial-assist knee orthosis with compact, backdrivable actuation," in *IEEE Int. Conf. Rehab. Robot.*, 2019, pp. 917–924.

[19] G. Lv and R. D. Gregg, "Underactuated potential energy shaping with contact constraints: Application to a powered knee-ankle orthosis," *IEEE Trans. Control Syst. Technol.*, vol. 26, no. 1, pp. 181–193, 2018.

[20] J. M. Hidler, M. Carroll, and E. H. Federovich, "Strength and coordination in the paretic leg of individuals following acute stroke," *IEEE Trans. Neural Syst. Rehabil. Eng.*, vol. 15, no. 4, 2007.

[21] S. S. Ng and C. W. Hui-Chan, "Contribution of ankle dorsiflexor strength to walking endurance in people with spastic hemiplegia after stroke," *Arch. Phys. Med. Rehab.*, vol. 93, no. 6, pp. 1046–1051, 2012.

[22] M. Yeatman, G. Lv, and R. D. Gregg, "Decentralized passivity-based control with a generalized energy storage function for robust biped locomotion," *J. Dynamic Systems, Measurement, and Control*, vol. 141, no. 10, p. 101007, 2019.

[23] R. M. Murray, Z. Li, and S. S. Sastry, *A Mathematical Introduction to Robotic Manipulation*. CRC press, 1994.

[24] G. Blankenstein, R. Ortega, and A. J. Van Der Schaft, "The matching conditions of controlled lagrangians and ida-passivity based control," *Int. J. Control*, vol. 75, no. 9, pp. 645–665, 2002.

[25] FlexiForce a401 sensor. [Online]. Available: http://www.tekscan.com/sites/default/files/resources/FLX-A401-G.pdf

[26] J. Yang and D. Winter, "Electromyographic amplitude normalization methods: improving their sensitivity as diagnostic tools in gait analysis," *Arch. Phys. Med. Rehab.*, vol. 65, no. 9, p. 517—521, 1984.

[27] K. R. Embry, D. J. Villarreal, R. L. Macaluso, and R. D. Gregg, "Modeling the kinematics of human locomotion over continuously varying speeds and inclines," *IEEE Trans. Neural Syst. Rehabil. Eng.*, vol. 26, no. 12, pp. 2342–2350, 2018.

[28] P. J. Millington, B. M. Myklebust, and G. M. Shambes, "Biomechanical analysis of the sit-to-stand motion in elderly persons," *Arch. Phys. Med. Rehab.*, vol. 73, no. 7, pp. 609–617, 1992.

[29] J. Pfusterschmied, T. Stöggl, M. Buchecker, S. Lindinger, H. Wagner, and E. Müller, "Effects of 4-week slackline training on lower limb joint motion and muscle activation," *J. Sci. Med. Sport*, vol. 16, no. 6, pp. 562–566, 2013.

[30] S. Nadeau, B. J. McFadyen, and F. Malouin, "Frontal and sagittal plane analyses of the stair climbing task in healthy adults aged over 40 years: what are the challenges compared to level walking?" *Clinical biomechanics*, vol. 18, no. 10, pp. 950–959, 2003.

[31] B. F. Mentiplay, M. Banky, R. A. Clark, M. B. Kahn, and G. Williams, "Lower limb angular velocity during walking at various speeds," *Gait & posture*, vol. 65, pp. 190–196, 2018.

[32] J. Lin, N. Divekar, G. Lv, and R. Gregg, "Energy shaping control with virtual spring and damper for powered exoskeletons," in *IEEE Conf. Decision & Control*, 2019.